A NEW MATHEMATICAL MODEL FOR DETERMINING FULL-ENERGY PEAK EFFICIENCY OF AN ARRAY OF TWO GAMMA DETECTORS COUNTING RECTANGULAR PARALLELEPIPED SOURCES

by

Mohamed S. BADAWI [1*], ***Mohamed E. KRAR*** [1], ***Ahmed M. EL-KHATIB*** [1], ***Slobodan I. JOVANOVIĆ*** [2, 3], ***Aleksandar D. DLABAČ*** [3], ***and Nikola N. MIHALJEVIĆ*** [3, 4]

[1] Department of Physics, Faculty of Science, Alexandria University, Alexandria, Egypt
[2] Department of Physics, Faculty of Mathematics and Natural Sciences, University of Montenegro, Podgorica, Montenegro
[3] Centre for Nuclear Competence and Knowledge Management, University of Montenegro, Podgorica, Montenegro
[4] Department of Mathematics, Maritime Faculty, University of Montenegro, Kotor, Montenegro

Scientific paper
DOI: 10.2298/NTRP1304370B

This work deals with full-energy peak efficiency for a counting array of two NaI(Tl) scintillation detectors (2 2 and 3 3 with 7.5% and 8.5% resolutions, respectively) and radioactive sources in the form of rectangular parallelepipeds of various dimensions. Aqueous solutions containing the ^{152}Eu radionuclide were used; the latter exhibits a favourable multiline gamma spectrum covering a wide energy range from121.78 keV up to 1408.03 keV. A new mathematical and analytical approach to the problem is developed. The well known, accurate and widely used efficiency transfer principle is applied, together with detector efficiency calculations based on the effective solid angle concept. The self-attenuation of the source matrix, attenuation by the source container and detector housing materials, as well as a number of other relevant details of the experimental set-up were duly accounted for. A remarkable agreement between the measured and calculated efficiencies was observed for a variety of source-to-detectors distances, confirming the reliability of the method developed.

Key words: effective solid angle, full-energy peak efficiency, gamma detector, rectangular parallelepiped source

INTRODUCTION

Full-energy peak efficiency (FEPE) is an important factor to be determined in a γ-spectroscopy system aiming to produce absolute measurements (*e. g.* interaction cross-section determination, quantitative elemental analysis, radioactivity measurements, *etc.*). Many researchers have applied Monte Carlo simulation software to solve the problem of efficiency calibration, either general purpose (*e. g.* PENELOPE, MCNP, and EGS) [1] or dedicated ones, such as GESEPCOR [2] or DETEFF [3]. Our radiation physics laboratory (Prof. Y. S. Selim Laboratory, Department of Physics, Faculty of Science, Alexandria University, Egypt) has previously developed a direct mathematical calculation method (DMC) based on exact mathematical modeling and expressions [4-10]. In this way, problems of efficiency calibration for different detectors were addressed for FEPE [4-7] and for total efficiency [8-10]. Unreliable specifications of detector parameters led to the use of optimized parameters instead of those provided by the manufacturers.

To cope with the sensitivity of the calculated FEPE to inaccurately report detector parameters (as is, to a lesser or greater degree, the case), the efficiency transfer (ET) principle was applied in the present work. FEPE values were calculated via effective solid angles by DMC. The counting arrangement considered includes an array of two γ-detectors and a rectangular parallelepiped source. The dimensions of both the detectors and the source are varied in subsequent validation exercises.

Moens [11] pioneered the efficiency transfer technique. It is based on the assumption that the ratio of the FEPE to the effective solid angle is independent of the sample geometry and composition for a given γ-ray energy and is, thus, an intrinsic property of the detector [12].

* Corresponding author; e-mail: ms241178@hotmail.com

The ET, as proposed by Moens and co-authors, is carried out according to the equation

$$\varepsilon_{\text{target}} \quad \frac{\Omega_{\text{target}}}{\Omega_{\text{ref}}} \varepsilon_{\text{ref}} \tag{1}$$

where $\varepsilon_{\text{target}}$ and ε_{ref}, are the FEPE for the γ-detector counting the target (point, plane, and volume) and reference geometry, respectively, while, Ω_{target} and Ω_{ref}, are the effective solid angles subtended by the detector surface with the target and the reference geometry, respectively. The two effective solid angles were computed by using the DMC. For the determination of the experimental reference efficiency, ε_{ref}, the efficiency transfer approach was used [13].

Making use of the ET technique, the present work assumes that: the FEPE of a system composed of two discrete detectors counting a rectangular parallelepiped radioactive source can be calculated based on the FEPE reference of the system with respect to a radioactive point source, so that

$$\varepsilon_{\text{rec}}^{\text{sys}}(E_\gamma) \quad \frac{\Omega_{\text{rec}}^{\text{sys}}(E_\gamma)}{\Omega_{\text{ref}}^{\text{sys}}(E_\gamma)} \varepsilon_{\text{ref}}^{\text{sys}}(E_\gamma) \tag{2}$$

where $\varepsilon_{\text{rec}}^{\text{sys}}(E_\gamma)$ and $\varepsilon_{\text{ref}}^{\text{sys}}(E_\gamma)$, are the FEPE for the two combined γ-ray detectors using a rectangular radioactive parallelepiped source and a radioactive point source as the reference geometry, respectively, while $\varepsilon_{\text{rec}}^{\text{sys}}(E_\gamma)$ and $\varepsilon_{\text{ref}}^{\text{sys}}(E_\gamma)$ are the effective solid angles subtended by the detector surface with the source and the reference geometry, respectively.

MATHEMATICAL ELABORATION

This section explains in detail the derivation of mathematical expressions used to calculate effective solid angles for point as well as for rectangular parallelepiped sources with respect to a cylindrical bi-detector system. The calculations take into account any attenuating material in between the source and the active material of the detection system, including the detector end-cap, holder and source container material, as well as source self-absorption.

Effective solid angle for a point source and a cylindrical detector

In a spherical co-ordinate system, the geometrical solid angle, $\Omega_{\text{geometrical}}$, subtended to a detector surface by an arbitrarily located radioactive point source [14, 15] is given by

$$\Omega_{\text{geometrical}} \quad \int_{\theta\ \varphi} \sin\theta \, \mathrm{d}\varphi \, \mathrm{d}\theta \tag{3}$$

where θ and φ are the polar and azimuthal angles, respectively, while the effective solid angle, $\Omega_{\text{effective}}$, is defined as

$$\Omega_{\text{effective}} \quad \int_{\theta\ \varphi} f_{\text{att}} \sin\theta \, \mathrm{d}\varphi \, \mathrm{d}\theta \tag{4}$$

where f_{att} is a factor for describing the attenuation of the incident radiation due to the different materials acting as attenuators between the source and the detector which can be expressed by the equation

$$f_{\text{att}} \quad \exp \quad \sum_{i\ 1}^{n} \mu_i d_i \tag{5}$$

where, μ_i is the total attenuation coefficient, without coherent scattering, of the i^{th} absorber for a γ-ray photon with energy, E_γ, its value obtained from [16]; d_i – the distance travelled in the material and, n, denotes the number of absorbers between the source and the detector's active material.

Considering a cylindrical detector denoted by cyl of radius R and depth L (see fig. 1), the effective solid angle, $\Omega_{\text{pnt}}^{\text{cyl}}(h,\rho,R)$, subtended to an arbitrary isotropic point source denoted by pnt above the detector surface by a distance h and displaced laterally by a distance ρ we obtain

$$\Omega_{\text{pnt}}^{\text{cyl}}(h,\rho,R) \quad \begin{array}{ll} 2\pi \int_0^{\theta_1} f_{\text{att}} \sin\theta \, \mathrm{d}\theta \quad 2 \int_{\theta_1}^{\theta_2} \int_0^{\varphi_{\max}} f_{\text{att}} \sin\theta \, \mathrm{d}\theta & \rho < R \\ \int_{\theta_1}^{\theta_2} \int_0^{\varphi_{\max}} f_{\text{att}} \sin\theta \, \mathrm{d}\theta & \rho \quad R \end{array} \tag{6}$$

with the attenuation factor, f_{att}, expressed as the product of two factors

$$f_{\text{att}} = f_{\text{hold}} \, f_{\text{cap}} \tag{7}$$

where f_{hold} and f_{cap} are the attenuation factors for the holder and end-cap, respectively, each dependent on both the energy and direction of the emerged photon, while the screening effect of the source and source container were neglected. So the, f_{hold}, can be represented by the equation

$$f_{\text{hold}} \quad \exp \quad \frac{\mu_{\text{hold}} \, t_{\text{hold}}}{\cos\theta} \tag{8}$$

where μ_{hold} is the total linear attenuation coefficient of the holder material t_{hold} – the thickness of the holder, and θ – the azimuthal angle.

Further, f_{cap}, can be expressed by the following multirange equation, where the representing expression is determined according to the values of θ , θ_{cap}, and φ_{cap}

$$f_{\text{cap}} \quad \begin{array}{llll} \exp & \frac{\mu_{\text{cap}} t_{\text{cap}}}{\cos\theta} & \theta_1 & \theta_{\text{cap}} \\ \exp & \frac{\mu_{\text{cap}} t_{\text{cap}}}{\cos\theta} & \varphi & \varphi_{\text{cap}}, \quad \theta_1 \quad \theta_{\text{cap}} \\ \exp & \frac{\mu_{\text{cap}} t_{\text{cap}}}{\sin\theta} & \varphi & \varphi_{\text{cap}}, \quad \theta_1 \quad \theta_{\text{cap}} \end{array} \tag{9}$$

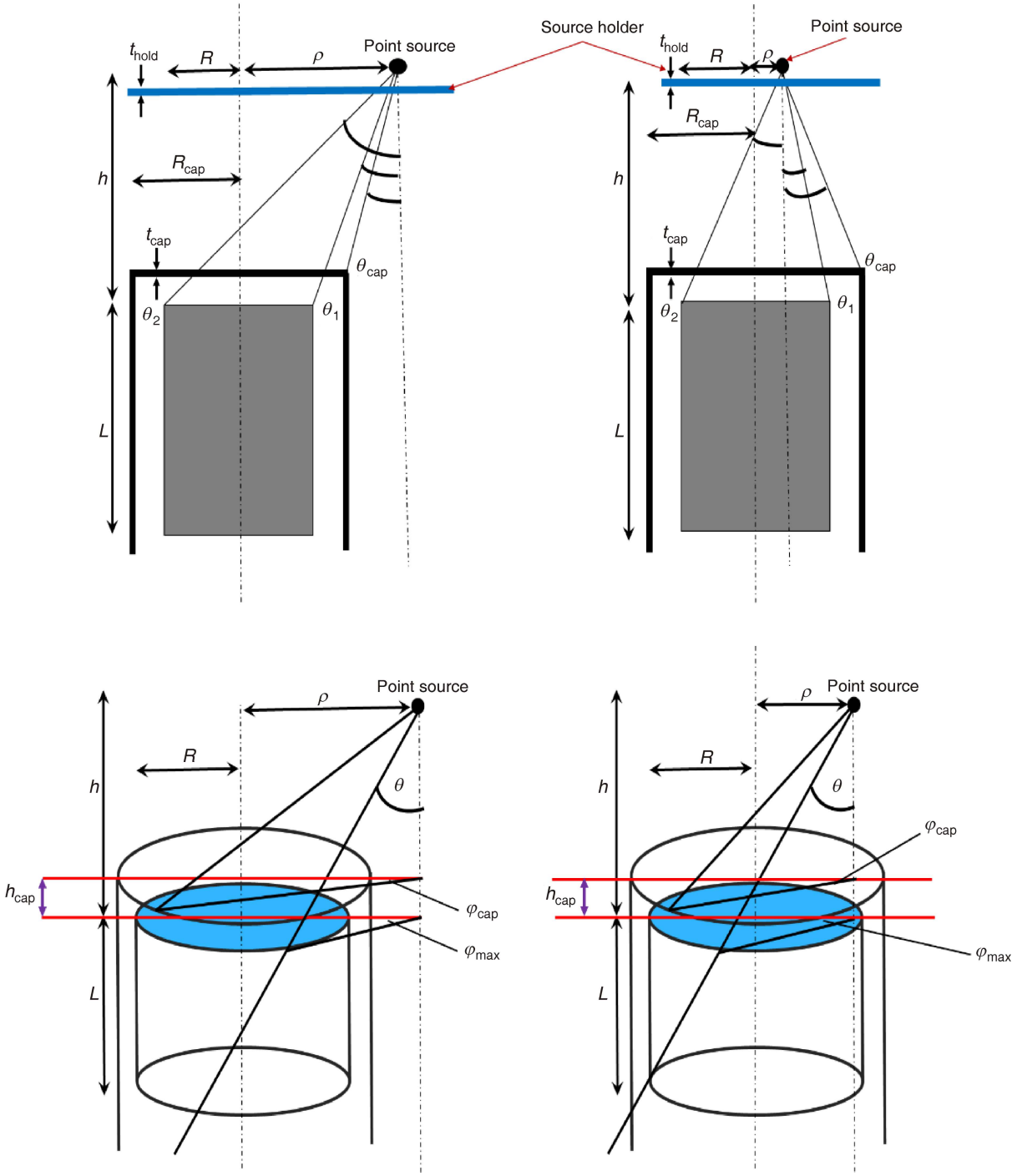

Figure 1. Arbitrarily located isotropic point source with a cylindrical detector for ρ R and $\rho < R$

where θ and φ are, the polar and azimuthal angles, respectively, of the direction of the emerged photon, while μ_{cap} and t_{cap}, are the total linear attenuation coefficients of the end-cap material and its thickness, respectively.

Where the maximum azimuth angle, φ_{max}, is given by the equation

$$\varphi_{max} \quad \cos^{1} \frac{\rho^2 \quad R^2 \quad h^2 \tan^2\theta}{2\rho h \tan\theta} \qquad (10)$$

and the polar angles are determined by

$$\theta_1 \quad \tan^{1} \frac{|R \quad \rho|}{h}, \quad \theta_2 \quad \tan^{1} \frac{R \quad \rho}{h} \qquad (11)$$

Effective solid angle using a point source with a bi-detector

A detection system composed of two discrete active material regions (detectors), in this instance, acting as a bi-detector system. Each region has a cylindri-

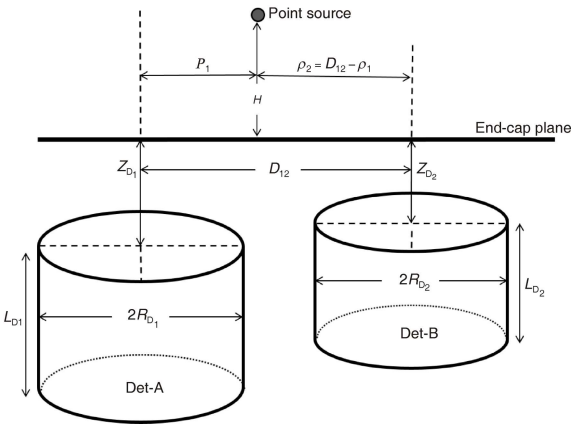

Figure 2. Schematic diagram of the bi-detector system with an arbitrary point source

cal shape with no restrictions on their dimensions, both are of a different size, while the separation between the two material regions can be arbitrarily chosen, as described in fig. 2.

The separation between the two cylindrical detectors represented by the axis-to-axis distances, D_{12}, R_{D_1}; R_{D_2}, denotes the detectors, Det-A, and, Det-B, radii, respectively, while L_{D_1} and L_{D_2}, denote their respective lengths. The system was arranged so that the end-caps surfaces of the detectors were placed in the same plane, while the detectors, Det-A, and, Det-B, surfaces were located at, Z_{D_1} and Z_{D_2}, under that plane, respectively.

The effective solid angle subtended by a radioactive isotropic point source and surfaces of the system composed of two detectors (bi-detectors, fig. 2), is expressed as the sum of effective solid angles subtended by the source and surfaces of each of the two detectors. The effective solid angle for the system, $\Omega^{sys}_{pnt}(h, \rho_1, R_1, R_2, D_{12})$, using an isotropic point source located at a distance H from the common end-cap and displaced laterally from the Det-A axis a distance ρ_1, is hence given as

$$\Omega^{sys}_{pnt}(H, \rho_1, R_1, R_2, D_{12}) \quad \Omega^{A}_{pnt}(H \quad Z_{D_1}, \rho_1, R_1) \quad \Omega^{B}_{pnt}(H \quad Z_{D_2}, D_{12} \quad \rho_1, R_2) \tag{12}$$

where Ω^{A}_{pnt} and Ω^{B}_{pnt} are the effective solid angles subtended by the surfaces of detectors Det-A and Det-B from the point source, respectively.

Effective solid angle using a rectangular parallelepiped with a bi-detector

Consider a rectangular parallelepiped source, fig. 3, its width denoted as W_S, its depth denoted as D_s,

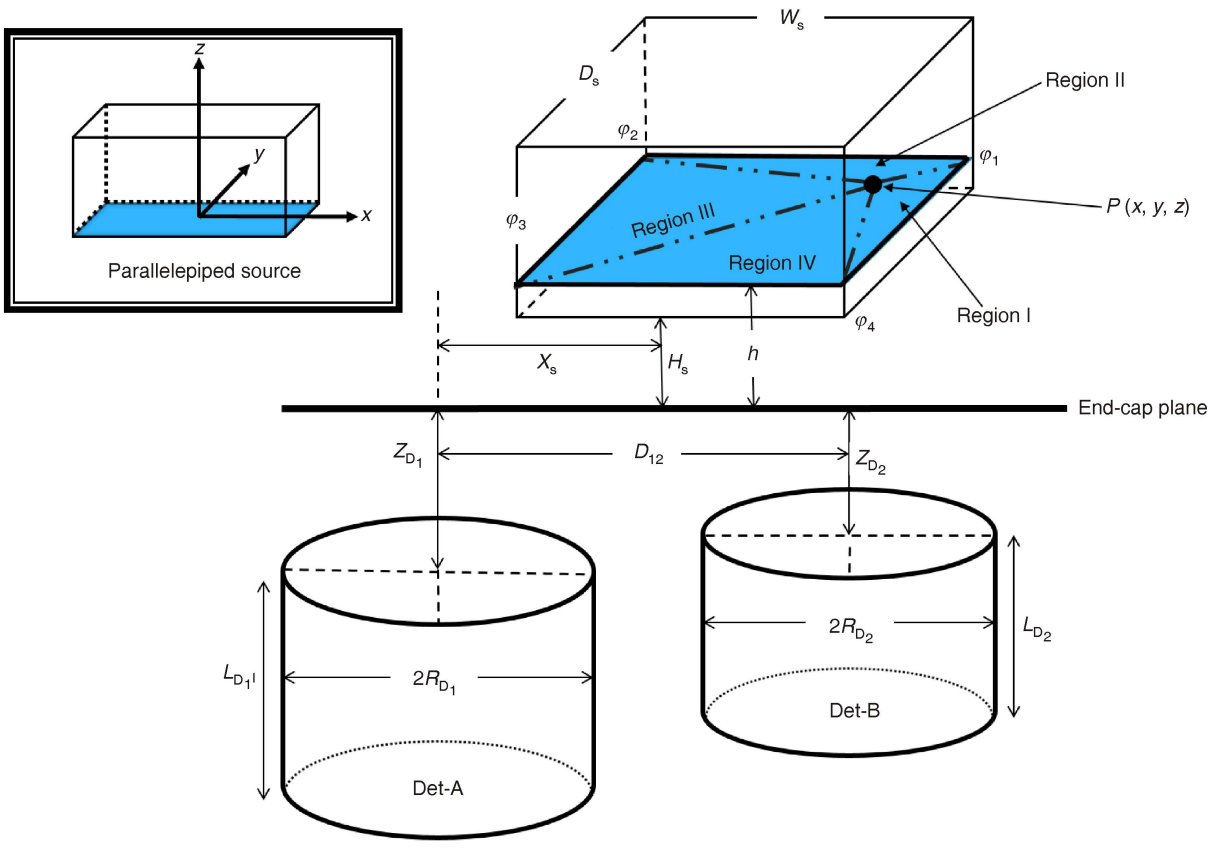

Figure 3. Schematic diagram of the bi-detector detection system with an arbitrarily located parallelepiped source

and its height denoted as L_s. The source is placed arbitrarily, so that its plane of symmetry is coincident with the plane of symmetry of the detection system. The source separated from the common end-cap is denoted by H_s, and its axis, lateral from, Det-A, is denoted as X_s.

According to [17, 18] treating a volumetric radioactive source as a group of point sources which are uniformly distributed. Similarly, using the appropriate Cartesian co-ordinate system, the effective solid angle of the volumetric rectangular parallelepiped source, $\Omega^{sys}_{rec}(W_s, D_s, L_s, X_s, H_s, Z_D)$, can be expressed by the integration

$$\Omega^{sys}_{rec}(W_s, D_s, L_s, X_s, H_s, Z_D) \quad \frac{2}{V}\int_{H_s}^{H_s}\int_{L_s}^{D_s/2}\int_{0}^{W_s/2}\Omega^{sys}_{pnt}(x, y, z)\,dx\,dy\,dz \tag{13}$$

where the integrand, $\Omega^{sys}_{pnt}(x, y, z)$, represents the effective solid angle of the system surface subtended by a point source located in the Cartesian co-ordinate, (x, y, z), as in fig. 3, represented by the equation

$$\Omega^{sys}_{pnt}(x, y, z) \quad \Omega^{A}_{pnt}(Z_{D_1} \quad H_s \quad z, \rho_1, R_1)\ \Omega^{B}_{pnt}(Z_{D_2} \quad H_s \quad z, D_{12} \quad \rho_2, R_2) \tag{14}$$

where, the lateral distances can be expressed in the Cartesian coordinate system by the equation

$$\rho_1 \quad \sqrt{(x_s \quad x)^2 \quad y^2},\ \rho_2 \quad \sqrt{(x_s \quad x)^2 \quad y^2} \tag{15}$$

where f_{att}, in eq. (6) represents the attenuation due to the source self-absorption and the other absorbers between the source and the detector, as given by the equation

$$f_{att} \quad f_s f_{con} f_{hold} f_{cap} \tag{16}$$

where, f_s, f_{con}, f_{hold}, and f_{cap} represent the attenuation due to the source, source container material, holder, and end-cap, respectively, each dependent on both the energy, as well as the direction of the emerged photon.

The attenuation due to holder material, f_{hold}, can be represented by the equation

$$f_{hold} \quad \exp\left(\frac{\mu_{hold}\, t_{hold}}{\cos\theta}\right) \tag{17}$$

where μ_{hold} is the total linear attenuation coefficient of the holder material and, t_{hold} – the thickness of the holder material, and θ – the polar angle while f_{cap} is expressed by the following multirange equations, according to the values of θ_1, θ_{cap}, and φ_{cap}.

$$f_{cap} \quad \begin{cases} \exp\left(\dfrac{\mu_{cap} t_{cap}}{\cos\theta}\right) & \theta_1 \quad \theta_{cap} \\ \exp\left(\dfrac{\mu_{cap} t_{cap}}{\cos\theta}\right) & \varphi \quad \varphi_{cap,}\ \theta_1 \quad \theta_{cap} \\ \exp\left(\dfrac{\mu_{cap} t_{cap}}{\sin\theta}\right) & \varphi \quad \varphi_{cap,}\ \theta_1 \quad \theta_{cap} \end{cases} \tag{18}$$

where θ and φ, are the polar and azimuthal angles, respectively, to the direction of the emerged photon; while μ_{cap} and t_{cap} represent the total linear attenuation coefficient of the end-cap material and its thickness, respectively.

The polar angle, θ_{cap}, is given by the equation

$$\theta_{cap} \quad \tan^{1}\frac{|R_{cap} \quad \rho|}{h \quad h_{cap}} \tag{19}$$

while the azimuthal angle, φ_{cap}, is given by the equation

$$\varphi_{cap} \quad \cos^{1}\frac{\rho^2 \quad R_{cap}{}^2 \quad (h \quad h_{cap})^2 \tan^2\theta}{2\rho(h \quad h_{cap})\tan\theta} \tag{20}$$

where R_{cap} and h_{cap} are the end-cap radius and its surface separation from the detector surface, respectively.

In addition, to express f_s and f_{con}, the azimuthal angle φ is divided into four regions, as depicted in fig. 3, bounded by the azimuthal angles stated by the equation

$$\varphi_1 \quad \tan^{1}\frac{\frac{1}{2}D_s \quad y}{\frac{1}{2}W_s \quad x},\ \varphi_2 \quad \tan^{1}\frac{\frac{1}{2}D_s \quad y}{\frac{1}{2}W_s \quad x}$$
$$\varphi_3 \quad \tan^{1}\frac{\frac{1}{2}D_s \quad y}{\frac{1}{2}W_s \quad x},\ \varphi_4 \quad \tan^{1}\frac{\frac{1}{2}D_s \quad y}{\frac{1}{2}W_s \quad x} \tag{21}$$

where

– Region I (0 $\varphi < \varphi_1$ or $\varphi_4 < \varphi < 2$)

$$f_s \quad \begin{cases} \exp\left(\dfrac{\mu_s z}{\cos\theta}\right) & \theta \quad \tan^{-1}\dfrac{\alpha}{z} \\ \exp\left(\dfrac{\mu_s \left(\frac{1}{2}W_s \quad x\right)}{\sin\theta}\right) & \theta \quad \tan^{-1}\dfrac{\alpha}{z} \end{cases} \tag{22}$$

$$f_{con} \quad \begin{cases} \exp\left(\dfrac{\mu_{con} t_{con}}{\cos\theta}\right) & \theta \quad \tan^{-1}\dfrac{\alpha}{z} \\ \exp\left(\dfrac{\mu_{con} t_{con}}{\sin\theta}\right) & \theta \quad \tan^{-1}\dfrac{\alpha}{z} \end{cases} \tag{23}$$

– Region II ($\varphi_1 \quad \varphi < \varphi_2$)

$$f_s \quad \exp\left(\frac{\mu_s z}{\cos\theta}\right) \quad \theta \quad \tan^{-1}\left(\frac{\beta}{z}\right) \quad \exp\left(\frac{\mu_s \left(\frac{1}{2}D_s \quad y\right)}{\sin\theta}\right) \quad \theta \quad \tan^{-1}\left(\frac{\beta}{z}\right) \tag{24}$$

$$f_{con} \quad \exp\left(\frac{\mu_{con} t_{con}}{\cos\theta}\right) \quad \theta \quad \tan^{-1}\left(\frac{\beta}{z}\right) \quad \exp\left(\frac{\mu_{con} t_{con}}{\sin\theta}\right) \quad \theta \quad \tan^{-1}\left(\frac{\beta}{z}\right) \tag{25}$$

– Region III ($\varphi_2 \quad \varphi \quad \varphi_3$)

$$f_s \quad \exp\left(\frac{\mu_s z}{\cos\theta}\right) \quad \theta \quad \tan^{-1}\left(\frac{\alpha}{z}\right) \quad \exp\left(\frac{\mu_s \left(\frac{1}{2}W_s \quad x\right)}{\sin\theta}\right) \quad \theta \quad \tan^{-1}\left(\frac{\alpha}{z}\right) \tag{26}$$

$$f_{con} \quad \exp\left(\frac{\mu_{con} t_{con}}{\cos\theta}\right) \quad \theta \quad \tan^{-1}\left(\frac{\alpha}{z}\right) \quad \exp\left(\frac{\mu_{con} t_{con}}{\sin\theta}\right) \quad \theta \quad \tan^{-1}\left(\frac{\alpha}{z}\right) \tag{27}$$

and

– Region IV ($\varphi_3 \quad \varphi < \varphi_4$)

$$f_s \quad \exp\left(\frac{\mu_s z}{\cos\theta}\right) \quad \theta \quad \tan^{-1}\left(\frac{\beta}{z}\right) \quad \exp\left(\frac{\mu_s \left(\frac{1}{2}D_s \quad y\right)}{\sin\theta}\right) \quad \theta \quad \tan^{-1}\left(\frac{\beta}{z}\right) \tag{28}$$

$$f_{con} \quad \exp\left(\frac{\mu_{con} t_{con}}{\cos\theta}\right) \quad \theta \quad \tan^{-1}\left(\frac{\beta}{z}\right) \quad \exp\left(\frac{\mu_{con} t_{con}}{\sin\theta}\right) \quad \theta \quad \tan^{-1}\left(\frac{\beta}{z}\right) \tag{29}$$

where μ_s and μ_{con} are the total linear attenuation coefficients without the coherent scattering for the source matrix and container material, respectively, while t_{con} is the container thickness, and parameters α and β are given by the equation

$$\alpha \quad \frac{\frac{1}{2}W_s \quad x}{\cos\varphi}, \quad \beta \quad \frac{\frac{1}{2}D_s \quad y}{\sin\varphi} \tag{30}$$

so, the FEPE of a system composed of two detectors using rectangular radioactive parallelepiped sources given by eq. (2) and eq. (12) and (13) can be calculated based on the FEPE reference of the system with respect to a radioactive point source as

$$\varepsilon_{rec}^{sys}(E_\gamma) \quad \frac{\Omega_{rec}^{sys}(W_s, D_s, L_s, X_s, H_s)}{\Omega_{pnt}^{sys}(h, \rho_1, R_1, R_2, D_{12})} \varepsilon_{pnt}^{sys}(E_\gamma) \tag{31}$$

EXPERIMENTAL SET-UP

Experimental measurements were done using a set of standard point sources obtained from PTB, Germany, and a set of rectangular homemade radioactive parallelepiped sources in different volumes. The certificates show the sources' activities and their uncertainties, as listed in tab. 1 and tab. 2. The data sheet states the values of half-life photon energies and photon emission probabilities per decay for all radionuclides used in the calibration process, as listed in tab. 3, which is available at the National Nuclear Data Center Web Page or on the IAEA website.

Table 1. PTB point sources' activities and their uncertainties

PTB-nuclide	Activity [kBq]	Reference date 00:00 hour	Uncertainty
^{152}Eu	290.0	June 1, 2009	1.38%
^{137}Cs	385.0		0.71%
^{60}Co	212.1		1.04%

Table 2. Characteristics of the rectangular parallelepiped sources

Standard source					Container	
ID	Length	Width	Height	Volume	Material	Thickness
V1	5.9 cm	3.8 cm	5.2 cm	100 mL	HDPE	0.15 cm
V2	6.1 cm	6.1 cm	6.2 cm	200 mL	PP	0.15 cm
Both have activity (5 kBq 1.98%, reference date January 1, 2010						

Table 3. Half-life, photon energies, and photon emission probabilities per decay for all radionuclides used in this work

PTB-nuclide	Energy [keV]	Emission probability [%]	Half-life [d]
^{152}Eu	121.78	28.4	4943.29
	244.69	7.49	
	344.28	26.6	
	778.9	12.96	
	964.13	14.0	
	1408.03	20.87	
^{137}Cs	661.66	85.21	11004.98
^{60}Co	1173.23	99.9	1925.31
	1332.5	99.982	

The detection system composed of two cylindrical NaI(Tl) scintillation detectors (Model 802 scintillation detectors, Canberra) of different sizes 3 3 (Det-A, fig. 4-A) and 2" 2" (Det-B, fig. 4-B). The de-

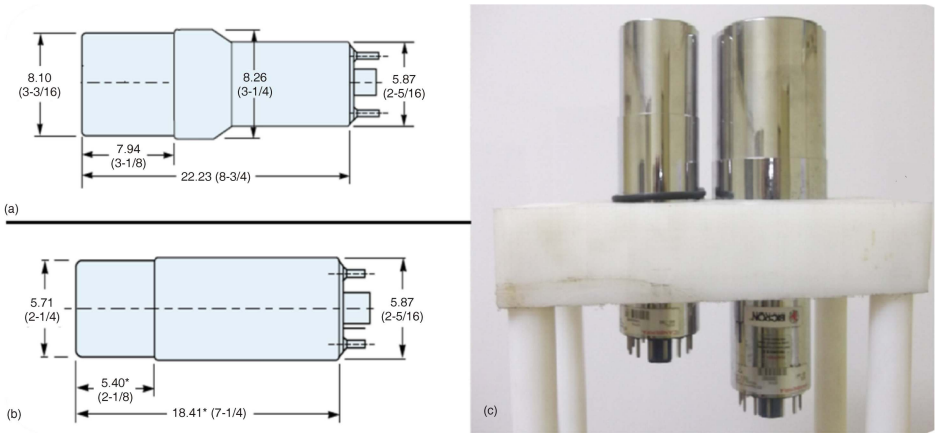

Figure. 4. (a) 3 3 detector, (b) 2 2 detector, and (c) mounting of the bi-detector system in a specially designed holder (dimensions in inches)

tectors mounted vertically in a specially constructed holder (fig. 4-c) made of teflon, so that the distance from side end-cap to side end-cap is 1cm. The details of the set-up parameters of the detectors, along with acquisition electronics specifications supported by the serial and model number, are listed in tab. 4.

Table 4. Detectors' set-up parameters with acquisition electronics specifications for detector (Det-A) and detector (Det-B)

Items	Detector Det-A	Detector Det-B
Manufacturer	Canberra	Canberra
Serial number	09L 652	09L 654
Detector model	802	802
Type	Cylindrical	Cylindrical
Mounting	Vertical	Vertical
Resolution (FWHM) at 661 [keV]	8.5%	7.5%
Cathode to anode voltage	+800 V DC	+900 V DC
Dynode to dynode	+80 V DC	+80 V DC
Cathode to dynode	+150 V DC	+150 V DC
Tube base	Model 2007	Model 2007
Shaping mode	Gaussian	Gaussian
Detector type	NaI(Tl)	NaI(Tl)
Crystal diameter [mm]	76.2	50.8
Crystal length [mm]	76.2	50.8
Top cover thickness [mm]	Al (0.5)	Al (0.5)
Side cover thickness [mm]	Al (0.5)	Al (0.5)
Reflector-oxide [mm]	2.5	2.5
Weight [kg]	1.8	0.77
Outer diameter [mm]	80.9	57.2
Outer length [mm]	79.4	53.9
Crystal volume [cm^3]	347.49	102.96

The measurements were done using radioactive sources placed at 30 cm above the detector common end-cap which allows to minimize the dead time to an order of zero and to neglect the effect of coincidence summing on experimental results, while all lateral distances are reported relative to the axis of the symmetry of Det-A.

The ^{152}Eu point source and homemade rectangular radioactive parallelepiped sources V1 and V2 were used to establish the experimental calibration curves in order to be compared with those calculated by the theoretical equations derived in this work. Besides that, two standard point sources, ^{60}Co and ^{137}Cs, were used for energy calibration and, at the time of acquisition, gain adjustment in both detectors done to make a match between the channels.

The measurements were carried out to obtain statistically significant main peaks in the spectra that are recorded and processed by winTMCA32 software made by ICx Technologies. The measured spectrum was saved in the form of spectrum ORTEC files which can be opened by ISO 9001 Genie 2000 data acquisition and analysis software made by Canberra. This acquisition time is high enough to get at least 20,000 counts, thus making the statistical uncertainties less than 0.5%. The typical acquisition time for a point source was several hours, as opposed to that of the volumetric sources which, due to the low activity, lasted at least 48 hours for each measurement. The spectra were analyzed with the program using its automatic peak search and peak area calculations, along with changes in the peak fit using the interactive peak fit interface when necessary to reduce the residuals and errors in peak area values. The peak areas, live time, run time, and the start time for each spectrum are entered into spreadsheets that are used to perform the calculations necessary to generate efficiency curves.

RESULTS AND DISCUSSION

The measured efficiency values as a function of the photon energy, $\varepsilon(E)$, for both NaI(Tl) scintillation detectors were calculated using the following formula

$$\varepsilon(E) \quad \frac{N(\mathrm{E})}{TA_{\mathrm{s}}P(\mathrm{E})} \quad C_{\mathrm{i}} \tag{32}$$

where N(E) is the number of counts in the full-energy peak obtained by using the Genie 2000 software, T – the measuring time (in seconds), P(E) – the photon emission probability at energy, E, obtained from the Genie 2000 standard library, while, A_{s} – the radionuclide activity, and C_{i}, represents the correction factors due to the dead time and radionuclide decay. No summing correc-

tion was done due to the very low dead time associated with the measurements and the corresponding correction factor for the dead time was obtained by simply using (ADC) live time. However, the background subtraction which was extremely important for low-activity rectangular sources was also carried out. The decay correction, C_d, for the calibration source from the reference time to the run time is given by

$$C_d \quad \exp(\lambda \Delta T) \tag{33}$$

where λ is the decay constant and T – the time interval over which the source is allowed to decay until the run time. The main source of uncertainty in the efficiency calculations were the uncertainties of the activities of the standard source solutions. The uncertainty in (FEPE), σ_ε, is given by

$$\sigma_\varepsilon \quad \varepsilon \sqrt{\frac{\sigma_N}{\partial N}^2 \quad \frac{\sigma_A}{\partial A}^2 \quad \frac{\sigma_P}{\partial P}^2} \tag{34}$$

where σ_N, σ_A, σ_P, are the uncertainties associated with the uncertainties in the quantities, N(E), A_S, and P(E), respectively.

The percentage deviations between the calculated and the measured full-energy peak efficiency values are calculated by

$$\Delta(\%) \quad \frac{\varepsilon_{cal} \quad \varepsilon_{meas}}{\varepsilon_{cal}} \quad 100 \tag{35}$$

where ε_{cal} and ε_{meas} are the calculated and the measured efficiencies, respectively.

All the integrals encountered are elliptic integrals which do not have a closed-form solution [19], so a numerical solution is obtained using the trapezoidal rule. Although the accuracy of the integration increases with the increase in the number of intervals n, the integration converges well at $n = 20$. A computer program (using the Microsoft QuickBasic Program) has been written to calculate the effective solid angles for arbitrarily located point and volumetric sources based on the derived equations.

The variations of the FEPE measured and calculated efficiencies based on eq. (31) of the bi-detector system, along with their associated uncertainties as a function of the photon energy using two volumetric rectangular parallelepiped sources (V1 and V2), are depicted in (figs. 5, 7, 9, 11, 13, and 15). These volumetric sources produced an energy range from 121.78 keV up to 1408.03 keV and placed it so that: its center is elevated 30 cm above the system's common end-cap, with a lateral displacement of 0 cm, 4.6 cm, and 8 cm, respectively.The difference in percentage between the FEPE measured and the calculated values as a function of the photon energy are presented in (figs. 6, 8, 10, 12, 14, and 16) for the bi-detectors and were found to amount to less than 6 [%]. The difference in the measured efficiencies themselves for dif-

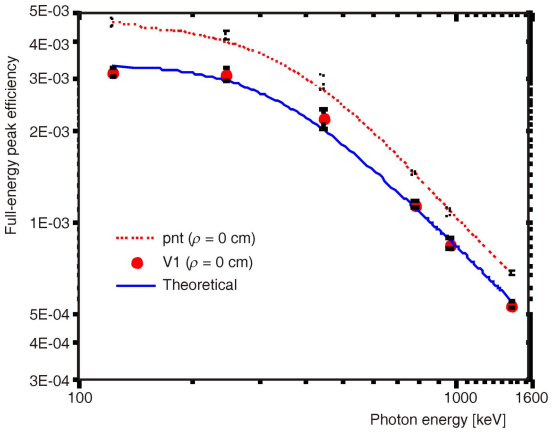

Figure 5. Calculated full-energy efficiency values and the measured ones with their associated uncertainties as a function of the photon energy for the bi-detector using a (V1) mounted axial to Det-A with its centers elevated 30 cm above the common end-cap plane and a point-like source at the (V1) center

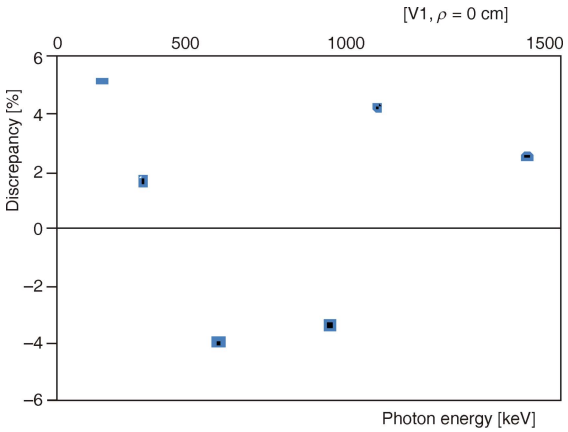

Figure 6. The difference percentage [%] calculated as a function of the photon energy for the bi-detector using a (V1) mounted axial to Det-A with its centers elevated 30 cm above the common end-cap

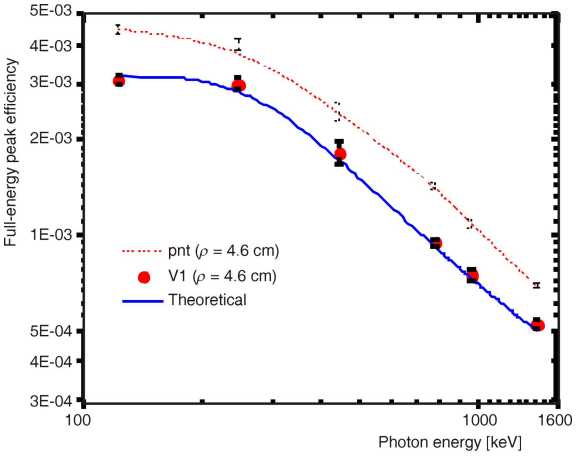

Figure 7. Calculated full-energy efficiency values and the measured ones, with their associated uncertainties as a function of the photon energy for the bi-detector using a (V1) mounted 4.6 cm lateral to Det-A with its centers elevated 30 cm above the common end-cap plane and a point-like source at the (V1) center

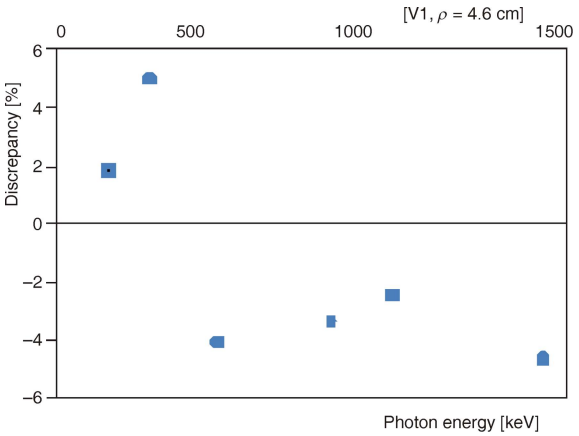

Figure 8. The difference percentage [%] calculated as a function of the photon energy for the bi-detector using a (V1) mounted 4.6 cm lateral to Det-A with its centers elevated 30 cm above the common end-cap plane

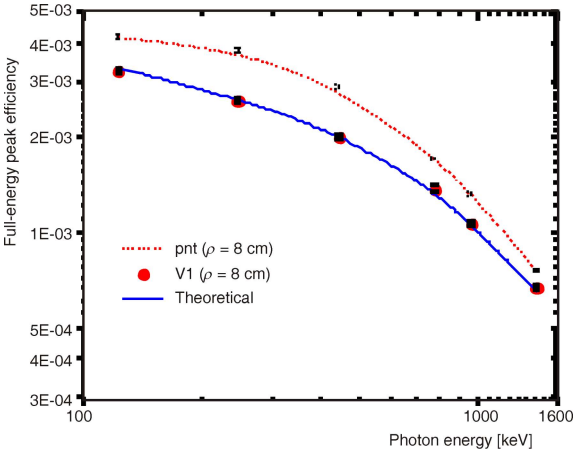

Figure 9. Calculated full-energy efficiency values and the measured ones, with their associated uncertainties as a function of the photon energy for the bi-detector using a (V1) mounted axial to Det-B with its centers elevated 30 cm above the common end-cap plane and a point-like source at the (V1) center

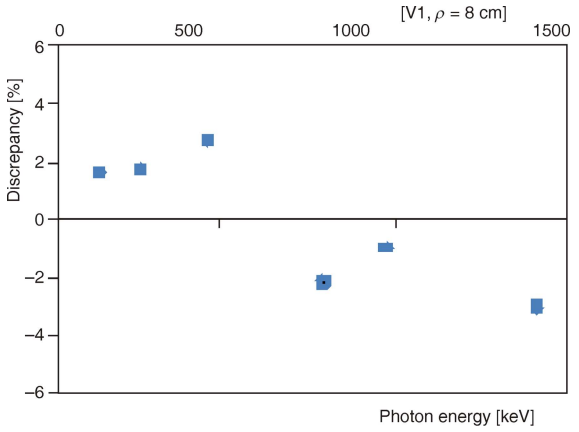

Figure 10. The difference percentage [%] calculated as a function of the photon energy for the bi-detector using a (V1) mounted axial to Det-B with its centers elevated 30 cm above the common end-cap plane

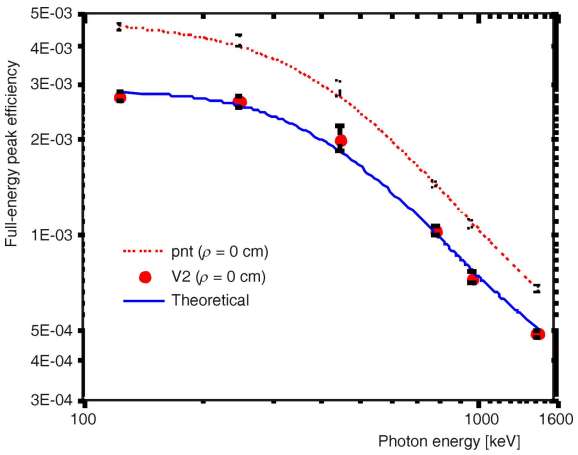

Figure 11. Calculated full-energy efficiency values and the measured ones, with their associated uncertainties as a function of the photon energy for the bi-detector using a (V2) mounted axial to Det-A with its centers elevated 30 cm above the common end-cap plane and a point-like source at the (V2) center

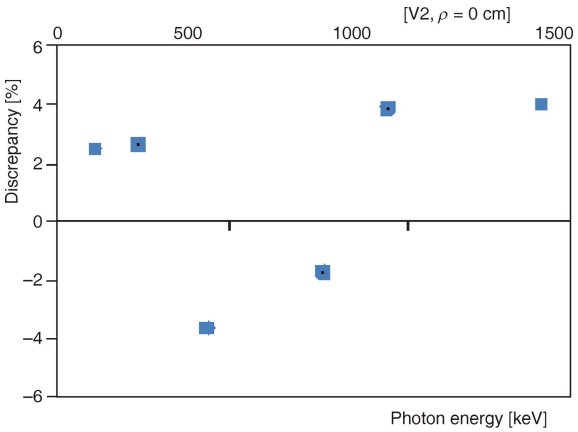

Figure 12. The difference percentage [%] calculated as a function of the photon energy for the bi-detector using a (V2) mounted axial to Det-A with its centers elevated 30 cm above the common end-cap plane

ferent source geometries relate to the sources used and can be mainly attributed to the self-absorption of the source, since a bigger volume is associated with lower efficiencies.

CONCLUSIONS

In the present work, the authors have introduced a new, simple numerical calculation method based on the ET technique over a wide energy range and an effective solid angle to evaluate the FEPE for a system combine of two γ-detectors. The factors related to photon attenuation in the detector end-cap, source container, source holder and the self-attenuation of the source have been derived and taken into account. The examination of the results obtained reveals a good agreement between the calculated and the measured

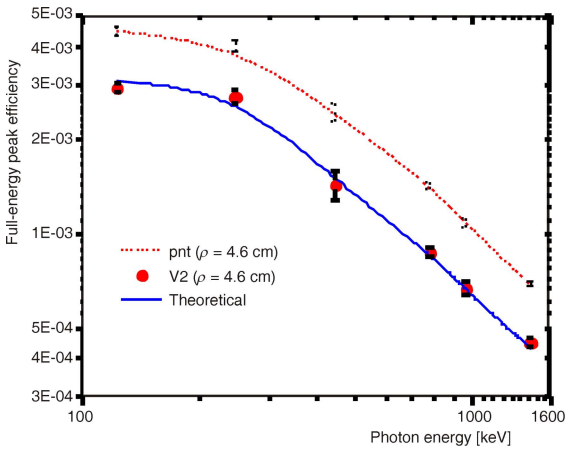

Figure 13. Calculated full-energy efficiency values and the measured ones, with their associated uncertainties as a function of the photon energy for the bi-detector using a (V2) mounted 4.6 cm lateral to Det-A with its centers elevated 30 cm above the common end-cap plane and a point-like source at the (V2) center

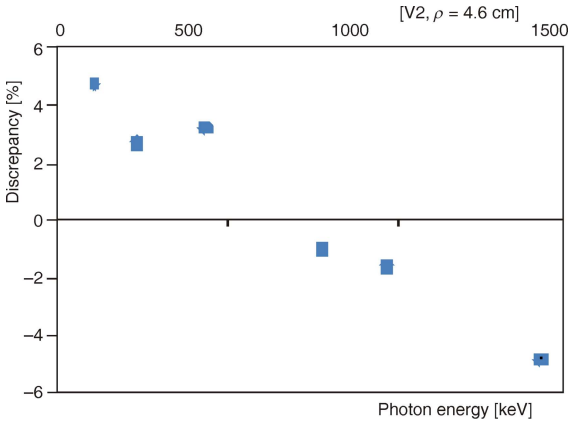

Figure 14. The difference percentage [%] calculated as a function of the photon energy for the bi-detector using a (V2) mounted 4.6 cm lateral to Det-A with its centers elevated 30 cm above the common end-cap plane

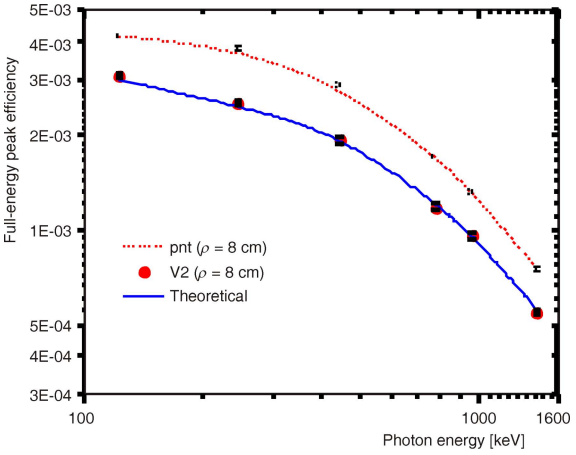

Figure 15. Calculated full-energy efficiency values and the measured ones, with their associated uncertainties as a function of the photon energy for the bi-detector using a (V2) mounted 8 cm lateral to Det-B with its centers elevated 30 cm above the common end-cap plane and a point-like source at the (V2)

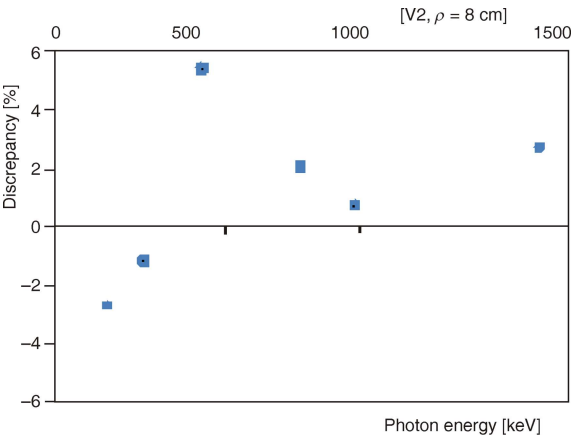

Figure 16. The difference percentage [%] calculated as a function of the photon energy for the bi-detector using a (V2) mounted 8 cm lateral to Det-B with its centers elevated 30 cm above the common end-cap plane

efficiencies and reflects the importance of considering attenuation factors in the study of detector efficiency. This study shows that the efficiency transfer technique can be used to evaluate the (FEPE) of a bi-detector system using rectangular parallelepiped sources. A remarkable agreement between the measured and calculated efficiencies for the bi-detector system at the source-to-system was verified by data comparison.

ACKNOWLEDGMENTS

The authors would like to express their sincere gratitude to Prof. Dr. Mahmoud I. Abbas, Faculty of Science, Alexandria University, for his valuable suggestions and collaboration. The authors would also like to express their thanks to The Physikalisch-Technische Bundesanstalt, Braunschweig, Berlin, Germany, for the outstanding help in preparing the homemade volumetric sources.

AUTHOR CONTRIBUTIONS

Mathematical and theoretical analysis was carried out by M. E. Krar, A. M. El-Khatib, and N. N. Mihaljević. The experiments were carried out by M. S. Badawi and M. E. Krar. All authors analyzed and discussed the results. The manuscript was written by M. S. Badawi and S. I. Jovanović. The figures were prepared by A. D. Dlabač and M. S. Badawi.

REFERENCES

[1] Vidmar, T., *et al.*, An Intercomparison of Monte Carlo Codes Used in Gamma-Ray Spectrometry, *Appl. Radiat. Isot., 66* (2008), 6-7, pp. 764-768
[2] Sima, O., Arnold, D., Dovlete, C., GESPECOR: A Versatile Tool in Gamma-Ray Spectrometry, *J. Radioanal. Nucl. Chem., 248* (2001), 2, pp. 359-364

[3] Díaz, N. C., Vargas, M. J., DETEFF: An Improved Monte Carlo Computer Program for Evaluating the Efficiency in Coaxial Gamma-Ray Detectors, *Nucl. Instrum. Methods. Phys. Res. A., 586* (2008), 2, pp. 204-210
[4] Abbas, M. I., Selim, Y. S., Bassiouni, M., HPGe Detector Photopeak Efficiency Calculation Including Self-Absorption and Coincidence Corrections for Cylindrical Sources Using Compact Analytical Expressions, *Radiat. Phys. Chem., 61* (2001), 3-6, pp. 429-431
[5] Abbas, M. I., Selim, Y. S., Calculation of Relative Full-Energy Peak Efficiencies of Well-Type Detectors, *Nucl. Instrum. Methods. Phys. Res. A., 480* (2002), 2-3, pp. 651-657
[6] Abbas, M. I., HPGe Detector Photopeak Efficiency Calculation Including Self-Absorption and Coincidence Corrections for Marinelli Beaker Sources Using Compact Analytical Expressions, *Appl. Radiat. Isot., 54* (2001), 5, pp. 761-768
[7] Abbas, M. I., Direct Mathematical Method for Calculating Full-Energy Peak Efficiency and Coincidence Corrections of HPGe Detectors for Extended Sources, *Nucl. Instrum. Methods. Phys. Res. A., 256* (2007), 1, pp. 554-557
[8] Abbas, M. I., Validation of Analytical Formulae for the Efficiency Calibration of Gamma Detectors Used in Laboratory and In-Situ Measurements, *Appl. Radiat. Isot., 64* (2006a), 12, pp. 1661-1664
[9] Abbas, M. I., Analytical Approach to Calculate the Efficiency of 4 NaI(Tl) Gamma-Ray Detectors for Extended Sources, *Nucl. Instrum. Methods. Phys. Res. A., 615* (2010), 1, pp. 48-52
[10] Selim, Y. S., Abbas, M. I., Direct Calculation of the Total Efficiency of Cylindrical Scintillation Detectors for Extended Circular Sources, *Radiat. Phys. Chem., 48* (1996), 1, pp. 23-27
[11] Mihaljević, N., Dlabač, A., Jovanović, S., Accounting for Detector Crystal Edge Rounding in Gamma-Efficiency Calculations, Theoretical Elaboration and Application in Angle Software, *Nucl Technol Radiat, 27* (2012), 1, pp. 1-12
[12] Vidmar, T., Likar, A., On the Invariability of the Total-To-Peak Ratio in Gamma-Ray Spectrometry, *Appl. Radiat. Isot., 60* (2004), 2-4, pp. 191-195
[13] Lepy, M. C., *et al*., Intercomparison of Efficiency Transfer Software for Gamma-Ray Spectrometry, *Appl. Radiat. Isot., 55* (2001), 4, pp. 493-503
[14] Gouda, M, M., *et al*., New Analytical Approach to Calculate the Co-Axial HPGe Detector Efficiency Using Parallelepiped Sources, *Journal of Advanced Rese. in Phys., 4* (2013), 1, 011303
[15] Badawi, M, S., *et al*., New Algorithm for Studying the Effect of Self Attenuation Factor on the Efficiency of [Gamma]-Rays Detectors, *Nucl. Instrum. Methods. Phys. Res. A., 696* (2012), pp. 164-170
[16] Hubbell, J. H., Seltzer, S. M., Tables of X-Ray Mass Attenuation Coefficients and Mass Energy-Absorption Coefficients 1 keV to 20 MeV for Elements $Z = 1$ to 92 and 48 Additional Substances of Dosimetric Interest, NISTIR-5632, USA, 1995
[17] Diab, S. M., *et al*., Computation of the Efficiency of NaI(Tl) Detectors Using Radioactive Inverted Well Beaker Sources Based on Efficiency Transfer Technique, *Journal of Advanced Rese. in Phys., 4* (2013), 1, 011301
[18] Badawi, M. S., *et al*., New Analytical Approach to Calibrate the Co-Axial HPGe Detectors Including Correction for Source Matrix Self-Attenuation, *Appl. Radiat. Isot., 70* (2012), 12, pp. 2661-2668
[19] Abbas, M. I., Analytical Calculations of the Solid Angles Subtended by a Well-Type Detector at Point and Extended Circular Sources, *Appl. Radiat. Isot., 64* (2006b), 9, pp. 1048-1056

Received on July 16, 2013
Accepted on September 19, 2013

**Мохамед С. БАДАВИ, Мохамед Е. КРАР, Ахмед М. ЕЛ-КАТИБ,
Слободан И. ЈОВАНОВИЋ, Александар Д. ДЛАБАЧ, Никола Н. МИХАЉЕВИЋ**

НОВИ МАТЕМАТИЧКИ МОДЕЛ ЗА ОДРЕЂИВАЊЕ ЕФИКАСНОСТИ СИСТЕМА ОД ДВА ГАМА ДЕТЕКТОРА И ИЗВОРЕ У ОБЛИКУ ПРАВОУГЛОГ ПАРАЛЕЛОПИПЕДА

У раду је приказан модел за одређивање ефикасности у пику пуне енергије система од два спрегнута NaI(Tl) сцинтилациона детектора (2 2 и 3 3 , са резолуцијом од 7.5% и 8.5%, респективно) и радиоактивне изворе у облику правоуглог паралелопипеда различитих димензија. Развијен је нови аналитички приступ, при чему је коришћен већ познати и поуздани принцип транфера ефикасности, уз рачунање ефикасности помоћу ефективног просторног угла. Овим је у потпуности узета у обзир атенуација у свим апсорберима (матрица и контејнер извора, конструкциони елементи детектора, елементи мерне конфигурације, итд.). Водени раствор радиоактивног изотопа ^{152}Eu, са прикладним спектром гама линија у широком опсегу (121.78 keV до 1408.03 keV) употребљен је за експерименталну проверу. Измерене вредности ефикасности веома се добро слажу са израчунатим, при различитим растојањима извор-детектори, чиме је потврђена поузданост методе.

Кључне речи: ефективни просторни угао, ефикасност система, гама детектор, правоугли паралелопипедни извор